J|A|C|S ARTICLES

Published on Web 07/22/2010

Neutral Transition Metal Hydrides as Acids in Hydrogen Bonding and Proton Transfer: Media Polarity and Specific Solvation Effects

Vladislava A. Levina,[†] Oleg A. Filippov,[†] Evgenii I. Gutsul,[†] Natalia V. Belkova,*[,†] Lina M. Epstein,[†] Agusti Lledos,[‡] and Elena S. Shubina*[,†]

A.N. Nesmeyanov Institute of Organoelement Compounds, Russian Academy of Sciences, Vavilov Street 28, 119991 Moscow, Russia, and Departament de Química, Universitat Autonoma de Barcelona, 08193 Bellaterra, Spain

Received May 6, 2010; E-mail: nataliabelk@ineos.ac.ru; shu@ineos.ac.ru

Abstract: Structural, spectroscopic, and electronic features of weak hydrogen-bonded complexes of $CpM(CO)_3H$ (M = Mo (**1a**), W (**1b**)) hydrides with organic bases (phosphine oxides R_3PO (R = *n*-C_8H_{17}, NMe_2), amines NMe_3, NEt_3, and pyridine) are determined experimentally (variable temperature IR) and computationally (DFT/M05). The intermediacy of these complexes in reversible proton transfer is shown, and the thermodynamic parameters ($\Delta H°$, $\Delta S°$) of each reaction step are determined in hexane. Assignment of the product ion pair structure is made with the help of the frequency calculations. The solvent effects were studied experimentally using IR spectroscopy in CH_2Cl_2, THF, and CH_3CN and computationally using conductor-like polarizable continuum model (CPCM) calculations. This complementary approach reveals the particular importance of specific solvation for the hydrogen-bond formation step. The strength of the hydrogen bond between hydrides **1** and the model bases is similar to that of the M−H···X hydrogen bond between **1** and THF (X = O) or CH_3CN (X = N) or between CH_2Cl_2 and the same bases. The latter competitive weak interactions lower the activities of both the hydrides and the bases in the proton transfer reaction. In this way, these secondary effects shift the proton transfer equilibrium and lead to the counterintuitive hampering of proton transfer upon solvent change from hexane to moderately polar CH_2Cl_2 or THF.

Introduction

Mechanistic investigations of proton transfer reactions involving transition metal hydrides are very important for catalysis, chemistry, and biochemistry.[1] In the past decade, it became well established that proton transfer from XH acids to transition metal hydrides proceeds through the stage of hydrogen-bond formation. In this case, hydrides serve as proton acceptors (bases), and dihydrogen-bonded $MH^{\delta-}\cdots H^{\delta+}X$ intermediates lead to cationic dihydrogen complexes $[M(\eta^2\text{-}H_2)]^+$ formation after proton transfer.[2−4] At the same time, many neutral hydrides possess another type of reactivity in proton transfer reaction, being rather strong acids.[5] Therefore, it was tenable to suppose the formation of hydrogen-bonded complex between a neutral hydride and a neutral base (B), $MH^{\delta+}\cdots B$, as an intermediate preceding proton transfer to organic bases. Indeed, we have found recently such a hydrogen bond between neutral hydrides $CpM(CO)_3H$ (**1**, M = Mo (a), W (b); Cp = η^5-C_5H_5) and organic bases.[6] This interaction could be important in catalytic pathways. It has been proposed that the marked deuterium isotope effects on optical yields found in asymmetric hydrogenations may be connected with the possibility of formation of a Rh−H···OMe hydrogen bond in the dihydride intermediate.[7] In very recent work,[8] the interaction of $CpMoH(CO)_3$ with catalytic cycle intermediate $(RCO)Rh(CO)_4$ has been suggested to be "the primary reason for the inhibition observed in the bimetallic catalytic hydroformylation" of alkenes.

The strength of the interaction between an acid AH and a base B and the position of proton between their electronegative atoms (eq 1) is widely accepted to depend on the acidity/basicity of the partners (proton affinity of A^- and B).[9] This is absolute for the gas phase, but in solution the solvents impose additional restraints. Thus, solvent effect becomes an important phenomenon in Bronsted acid−base systems influencing the intracomplex proton transfer reaction (eq 1).

[†] Russian Academy of Sciences.
[‡] Universitat Autonoma de Barcelona.

(1) *Recent Advances in Hydride Chemistry*; Peruzzini, M., Poli, R., Eds.; Elsevier: Amsterdam, 2001; p 580.
(2) Belkova, N. V.; Shubina, E. S.; Epstein, L. M. *Acc. Chem. Res.* **2005**, *38*, 624–631.
(3) Epstein, L. M.; Shubina, E. S. *Coord. Chem. Rev.* **2002**, *231*, 165–181.
(4) Besora, M.; Lledós, A.; Maseras, F. *Chem. Soc. Rev.* **2009**, *38*, 957–966.
(5) Kristjánsdóttir, S. S.; Norton, J. R. In *Transition Metal Hydrides*; Dedieu, A., Ed.; VCH: New York, 1991; pp 309−359.
(6) Belkova, N. V.; Gutsul, E. I.; Filippov, O. A.; Levina, V. A.; Valyaev, D. A.; Epstein, L. M.; Lledós, A.; Shubina, E. S. *J. Am. Chem. Soc.* **2006**, *128*, 3486–3487.
(7) Imamoto, T.; Itoh, T.; Yoshida, K.; Gridnev, I. D. *Chem. Asian J.* **2008**, *3*, 1636–1641.
(8) Li, C.; Cheng, S.; Tjahjono, M.; Schreyer, M.; Garland, M. *J. Am. Chem. Soc.* **2010**, *132*, 4589–4599.
(9) Chan, B.; Del Bene, J. E.; Elguero, J.; Radom, L. *J. Phys. Chem. A* **2005**, *109*, 5509–5517.

10.1021/ja103862r

$$AH\cdots B \rightleftarrows A^{-}\cdots {}^{+}HB \quad (1)$$

Even subtle changes in the environment could drive the equilibrium shift toward the hydrogen-bonded ion pair. In a hydrogen-bond-donating media (SH), a cooperative interaction (eq 2) evokes an enhancement of the ROH···N hydrogen-bond strength and distinctly favors the proton transfer.[10−16] Competition of solvent functionalities and reaction partners in hydrogen bonding and proton transfer of many organic systems has been discussed nicely by Hunter.[17]

$$\mathrm{SH{-}{-}{-}OH{-}{-}{-}NR_3} \rightleftharpoons \mathrm{SH{-}{-}{-}O^{-}{-}{-}NR_3} \quad (2)$$

Recently, we have shown[18] that the cooperative effect of binding of the second ROH molecule or the hydrogen-bond-donating solvent facilitates the proton transfer within dihydrogen bond Ru−H···HOR, whereas hydrogen-bond-accepting solvents hamper the process by lowering the ROH activity. These effects are found particularly important at rather low media polarity.[18] Similarly, the deactivating effect of acetonitrile relative to CH_2Cl_2 on the reaction of $[W_3PdS_4H_3(dmpe)_3(CO)]^+$ cubane cluster with HCl was explained by the formation of a strong $ClH\cdots NCCH_3$ bond, which cannot be compensated with the stabilization achieved with formation of a dihydrogen bond.[19]

In this Article, we present the full report on the spectroscopic and theoretical investigation of the structure, electron distribution, and thermodynamics of the intermolecular hydrogen-bonded complexes MH···B and the detailed study of proton transfer to different organic bases (Scheme 1) in various solvents with the emphasis on the analysis of nonspecific and specific solvent effects.

Experimental Section

The molybdenum and tungsten hydrides **1** were prepared as previously described.[20] All samples for IR studies were prepared under a dry argon atmosphere using standard Schlenk techniques. The solvents and liquid bases used were purified by refluxing over Na (hexane), Na/benzophenone (THF), and CaH_2 (CH_2Cl_2, CH_3CN, hexamethylphosphoramide (HMPA), and pyridine) and were distilled prior to use under a dry argon atmosphere.

Molybdenum hydride **1a** loses Cp ring as a result of interaction with acetonitrile at room temperature, but the reaction becomes slow enough below 270 K[21] to not interfere with the study performed within ca. 10 h. However, at 230 K slow proton transfer from **1a** to the solvent occurs (see Results). For this reason, the bases (or their solutions) were added to the freshly made acetonitrile solution of **1a** at 230 K before the hydride dissociation became visible. Tungsten hydride **1b** is stable in acetonitrile in the whole range of temperatures used in this work.

Scheme 1

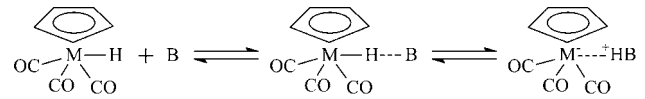

Low temperature IR measurements were carried out using an "Infralum FT-801" spectrometer and a Carl Zeiss Jena cryostat in the temperature range 180−300 K under a stream of liquid nitrogen. The accuracy of the experimental temperature adjustment was ±1 K. The CaF_2 cells of 0.04 or 0.12 cm width were used.

The dielectric permittivity ε of all of the solvents used increases with the temperature decrease and was calculated as in refs 22−25.

The proton-accepting ability (E_j) of hexamethylphosphoramide (HMPA) was calculated using the empirical "rule of factors" (eq 3),[26] where E_j is the proton-accepting ability of a base (HMPA), P_i is the proton-donating ability of an acid (CH_3OH, $P_i = 0.63$[26]), ΔH_{11} is the enthalpy of the hydrogen-bond formation between phenol and diethyl ether (standard pair), which is −5.7 kcal mol^{-1} for hexane,[26] and ΔH_{ij} is the experimental enthalpy of the hydrogen-bond formation between HMPA and methanol, which was obtained using the correlation equation (eq 4),[27,28] where $\Delta\nu_{OH} = 268$ cm^{-1}):

$$P_i = \Delta H_{ij}/(\Delta H_{11} E_j) \quad (3)$$

$$-\Delta H^{o} = 18\Delta\nu_{OH}/(\Delta\nu_{OH} + 720) \quad (4)$$

The proton-donating ability (P_i) of hydrides **1** was calculated using eq 3, where E_j is the proton-accepting ability of a base (HMPA, $E_j = 1.36$), and P_i is the proton-donating ability of an acid (hydrides **1**).

Computational Details

All calculations were performed at the DFT level, by means of the M05 functional[29] as implemented in Gaussian 03.[30] The Mo and W atoms were described by the LANL2TZ(f) basis set,[31] which is an uncontracted version of LANL2DZ and includes an f polarization function and an ECP.[32,33] The 6-31G(d,p) basis set was used for all other atoms except hydride ligand, which was associated with the 6-311++G(d,p) basis set. The structures of the reactants, intermediates, transition states, and products were fully optimized without any symmetry restriction. Transition states were identified by having one imaginary frequency in the Hessian matrix. IRC calculations were carried out in both directions starting from the located transition states. No scaling factor was applied to the

(10) Kuc, T.; Pawelka, Z. *J. Solution Chem.* **2001**, *30*, 375–387.
(11) Kuc, T.; Pawelka, Z.; Sobczyk, L. *Phys. Chem. Chem. Phys.* **2000**, 211–216.
(12) Kuc, T.; Zeegers-Huyskens, T.; Pawelka, Z. *J. Mol. Liq.* **2000**, *89*, 147–158.
(13) Kuc, T.; Pawelka, Z.; Sobczyk, L. *Phys. Chem. Chem. Phys.* **2001**, *3*, 5201–5207.
(14) Fritsch, J.; Zundel, G. *J. Phys. Chem.* **1981**, *85*, 556–561.
(15) Kraemer, R.; Zundel, G. *J. Chem. Soc., Faraday Trans.* **1990**, *86*, 301–305.
(16) Zundel, G.; Fritsch, J. *J. Phys. Chem.* **1984**, *88*, 6295–6302.
(17) Hunter, C. A. *Angew. Chem., Int. Ed.* **2004**, *43*, 5310–5324.
(18) Belkova, N. V.; Gribanova, T. N.; Gutsul, E. I.; Minyaev, R. M.; Bianchini, C.; Peruzzini, M.; Zanobini, F.; Shubina, E. S.; Epstein, L. M. *J. Mol. Struct.* **2007**, *844*, 115–131.
(19) Algarra, A. G.; Basallote, M. G.; Feliz, M.; Fernández-Trujillo, M. J.; Llusar, R.; Safont, V. S. *Chem.-Eur. J.* **2010**, *16*, 1613–1623.
(20) Herrmann, W. A.; Bauer, G. *Synthetic Methods of Organometallic and Inorganic Chemistry, Part 2 Transition Metals*; Georg Thieme Verlag: Stuttgart, 1997; Vol. 8, p 90.
(21) Jordan, R. F.; Norton, J. R. *J. Am. Chem. Soc.* **1982**, *104*, 1255–1263.
(22) Morgan, S. O.; Lowry, H. H. *J. Phys. Chem.* **1930**, *34*, 2385–2432.
(23) Metz, D. J.; Glines, A. *J. Phys. Chem. A* **1967**, *71*, 1158.
(24) Carvajal, C.; Tolle, K. J.; Smid, J.; Szwarc, M. *J. Am. Chem. Soc.* **1965**, *87*, 5548.
(25) Cote, J.-F.; Broullette, D.; Desnoyers, J. E.; Rouleau, J.-F.; St-Arnaud, J.-M.; Perron, G. *J. Solution Chem.* **1996**, *25*, 1163.
(26) Iogansen, A. V. *Theor. Exp. Chem.* **1971**, *7*, 302–311.
(27) Iogansen, A. V. *Spectrochim. Acta, Part A* **1999**, *55*, 1585–1612.
(28) Iogansen, A. V. *Opt Spectrosc.* **1967**, *3*, 228.
(29) Zhao, Y.; Schultz, N. E.; Truhlar, D. G. *J. Chem. Phys.* **2005**, *123*, 161103.
(30) Frisch, M. J.; et al. *Gaussian 03*, revision E.01; Gaussian, Inc.: Wallingford, CT, 2004.
(31) Roy, L. E.; Hay, P. J.; Martin, R. L. *J. Chem. Theory Comput.* **2008**, *4*, 1029–1031.
(32) Hay, P. J.; Wadt, W. R. *J. Chem. Phys.* **1985**, *82*, 270–283.
(33) Wadt, W. R.; Hay, P. J. *J. Chem. Phys.* **1985**, *82*, 284–298.

Table 1. Basicity Factors (E_j) and Conjugated Acid Acidities ($pK_a(BH^+)$) of the Bases Employed

	E_j	$pK_a(BH^+)$ in CH_3CN	$pK_a(BH^+)$ in THF
HMPA	1.36[a]	6.1[42 b]	2.1[43]
Py	1.30[26]	12.5[44]	5.5[45]
NEt_3	1.70[26]	18.8[46]	12.5[45]

[a] This work. [b] In CH_3NO_2.

calculated frequencies because the optimization was run in the gas phase and the IR spectra were measured in solution. Nonspecific solvent effects were introduced through CPCM[34,35] continuum representation of the solvent by single-point calculations on gas-phase-optimized geometries for acetonitrile ($\varepsilon = 36.64$), dichloromethane ($\varepsilon = 8.93$), THF ($\varepsilon = 7.58$), and heptane ($\varepsilon = 1.92$). The energies in solvent have been obtained by adding the contribution of the free energy of solvation to the gas-phase potential energy. Topological analysis of the electron density distribution function $\rho(r)$ was performed using the AIMALL program package[36] based on the wave function obtained by the M05 single-point calculations on previously optimized geometries with substitution of effective core potential LANL2TZ(f) basis set by all electron WTBS basis set.[37,38] The energy of the hydrogen-bonding interaction was estimated using the correlation between the energy of the contact (E_{cont}) and the value of the potential energy density function $V(r)$ in (3,−1) critical point: $E_{cont} = {}^1/_2V(r)$.[39,40]

The gas-phase proton affinity (PA) calculated as $-\Delta H_{298.15K}$ for the reaction $B + H^+ \rightarrow BH^+$ is 224.5 kcal mol^{-1} for Py, 224.9 kcal mol^{-1} for Me_3PO, 226.0 kcal mol^{-1} for Me_3N, 321.6 kcal mol^{-1} for $[CpMo(CO)_3]^-$, and 327.1 kcal mol^{-1} for $[CpW(CO)_3]^-$.

Results

1. Hydrogen Bonds between Hydrides 1 and Bases (in Hexane). Three compounds possessing different basicity (pK_a) and proton-accepting ability in hydrogen bonding (E_j, Table 1) were chosen as proton acceptors: pyridine (Py), triethylamine (NEt_3), and hexamethylphosphoramide (HMPA). The peculiarity of HMPA is that the hydrogen-bond formation constant for this base is often 2−3 times greater than in the case of the other proton acceptors.[41]

IR spectra of **1** feature two characteristic ν_{CO} bands. The lower frequency band is broader and has nonsymmetric shape due to overlap of the asymmetric stretching vibrations ν^2_{CO} (A″) and ν^3_{CO} (A′).[47,48] The high frequency band ν^1_{CO} is assigned to symmetric stretching vibration of CO groups A′. The position of the low frequency ν_{CO} band depends slightly on temperature, shifting to lower frequencies upon cooling (see the Supporting Information for details) with the concomitant increase in the intensity of both bands. The bands of M−H stretching vibrations (ν_{MH}) of **1a** and **1b** are located at lower frequencies (1785 and 1846 cm^{-1}, respectively) and have much lower intensity. MH···B hydrogen-bond formation induces lower frequency shift of both ν_{CO} (Figure S1[49]) and ν_{MH} (Figure 1) stretches with respect to free hydride **1**.[6] In the ν_{MH} range, the increase of the base (HMPA and $Oc_3P{=}O$ (Oc = n-C_8H_{17})) excess causes the progressive shift of the ν_{MH} bands to lower frequencies ($\Delta\nu_{MH}$ = up to −20 cm^{-1}) (Figure 1), because very broad ν_{MH}(free) and ν_{MH}(bonded) bands overlap and the spectra reveal the envelope of the two bands. Analogous IR spectral changes have been observed for hydrogen bonds of phosphine oxides with cationic hydride $[Cp^*_2OsH]^+\cdots O{=}PR_3$.[50]

The use of phosphine oxides for MH···B hydrogen-bond formation studies is especially effective due to the presence of an additional spectral label, the $\nu_P{=}O$ band. This band is quite sensitive to the interaction, shifting to lower frequencies in the case of hydrogen bonding with organic acids, $XH\cdots O{=}PR_3$.[51,52]

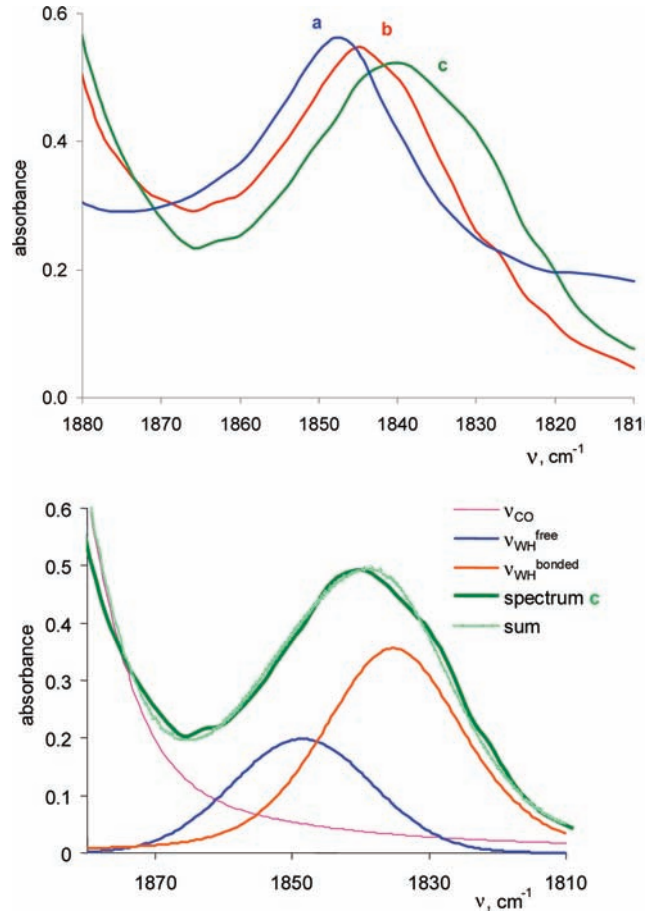

Figure 1. Top: IR spectra (ν_{MH} range) of $CpW(CO)_3H$ (0.0025 M (a), blue) in the presence of Oc_3PO (0.0125 M (b), red; 0.025 M (c), green). Hexane, 290 K. l = 0.22 cm. Bottom: Band decomposition analysis for spectrum c.

(34) Barone, V.; Cossi, M. *J. Phys. Chem. A* **1998**, *102*, 1995–2001.
(35) Cossi, M.; Rega, N.; Scalmani, G.; Barone, V. *J. Comput. Chem.* **2003**, *24*, 669–681.
(36) Keith, T. A. *AIMAll*, 2009; aim.tkgristmill.com.
(37) Huzinaga, S.; Miguel, B. *Chem. Phys. Lett.* **1990**, *175*, 289–291.
(38) Huzinaga, S.; Klobukowski, M. *Chem. Phys. Lett.* **1993**, *212*, 260–264.
(39) Espinosa, E.; Molins, E.; Lecomte, C. *Chem. Phys. Lett.* **1998**, *285*, 170–173.
(40) Espinosa, E.; Alkorta, I.; Rozas, I.; Elguero, J.; Molins, E. *Chem. Phys. Lett.* **2001**, *336*, 457–461.
(41) Abraham, M.; Grelier, P.; Prior, D. V. *Tetrahedron Lett.* **1989**, *30*, 2571.
(42) Matrosov, E. I.; Tsvetkov, E. N.; Mironova, Z. N.; Malevannaya, R. A.; Kabachnik, M. I. *Izv. USSR, Ser. Khim.* **1975**, 1333.
(43) Abdur-Rashid, K.; Fong, T. P.; Greaves, B.; Gusev, D. G.; Hinman, J. G.; Landau, S. E.; Lough, A. J.; Morris, R. H. *J. Am. Chem. Soc.* **2000**, *122*, 9155–9171.
(44) Coetzee, J. F.; Padmanobhan, G. R. *J. Am. Chem. Soc.* **1965**, *87*, 5005–5010.
(45) Rõõm, E.-I.; Kütt, A.; Kaljurand, I.; Koppel, I.; Leito, I.; Koppel, I. A.; Mishima, M.; Goto, K.; Miyahara, Y. *Chem.-Eur. J.* **2007**, *13*, 7631.
(46) Kaljurand, I.; Kutt, A.; Soovali, L.; Rodima, T.; Maemets, V.; Leito, I.; Koppel, I. A. *J. Org. Chem.* **2005**, *70*, 1019–1028.
(47) Davidson, G.; Duce, D. A. *J. Organomet. Chem.* **1976**, *120*, 229.
(48) Hooker, R. H.; Rest, A. J. *J. Organomet. Chem.* **1982**, *234*, C23.
(49) Interestingly, the $\nu_{CO}{}^{as}$ band is more sensitive to hydrogen-bond formation ($\Delta\nu_{CO} = \nu_{CO}$(complex) $-\nu_{CO}$(free) = −4 to −12 cm^{-1}) than is the high frequency $\nu_{CO}{}^{s}$ band ($\Delta\nu \approx 4$ cm^{-1}).
(50) Shubina, E. S.; Krylov, A. N.; Kreindlin, A. Z.; Rybinskaya, M. I.; Epstein, L. M. *J. Organomet. Chem.* **1993**, *447*, 277–280.

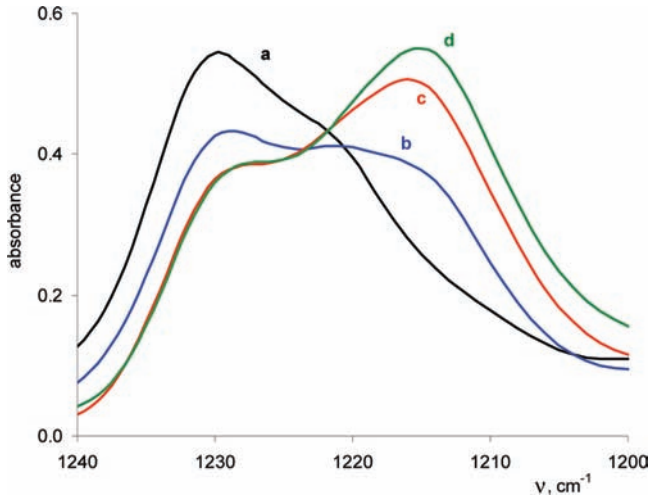

Figure 2. IR spectra (ν_{PO} range) of HMPA (0.005 M, 290 K) (a), in the presence of $CpW(CO)_3H$ (0.06 M) at different temperatures: 290 K (b), 250 K (c), and 260 K (d). $l = 0.12$ cm.

Table 2. Thermodynamic Characteristics of Hydrogen-Bonded Complexes of **1** with HMPA in Hexane

M	pK_a (in MeCN)[21]	pK_a (in THF)[45]	$\Delta H_{1-2}°$ (kcal mol^{-1})	$\Delta S_{1-2}°$ (eu)	P_i
Mo **1a**	13.9	17	-3.2 ± 0.6	-10 ± 2	0.44
W **1b**	16.1	18.6	-2.4 ± 0.6	-5 ± 2	0.35

The addition of an excess of hydrides **1a** or **1b** to the hexane solution of HMPA ($c = 0.01$ M) leads to the appearance of a new low frequency ν_{PO}(bonded) band, whose intensity grows with the decrease of temperature (Figure 2). The same changes were observed with the increase of the hydride excess (0.05−0.2 M). The band shift, $\Delta\nu_{PO} = \nu_{PO}$(bonded) $- \nu_{PO}$(free), varies from -10 to -14 cm^{-1} depending on the nature of hydride and phosphine oxide. All spectral changes are more significant in the case of **1a** than **1b**, correlating with the greater acidity (pK_a) of the former.[21]

The high sensitivity of the ν_{PO} and ν_{CO} bands allowed us to obtain reliable quantitative characteristics of the MH···O═P hydrogen bond. The hydrogen-bond formation constants, K_{1-2}, were calculated from the ν_{PO} or ν_{CO} band intensity changes upon hydrogen-bond formation relative to that of free HMPA or **1**, respectively. The thermodynamic parameters ($\Delta H°$, $\Delta S°$, see Table 2) were obtained from the K_{1-2} temperature dependence. Using the empirical "rule of factors",[26] the proton-donating ability (P_i) of hydrides could be estimated from the $-\Delta H°$ values by eq 3.

The lower basicity in hydrogen bonding and generally lower hydrogen-bond formation constants for pyridine relative to HMPA necessitated the use of higher excess of this base (10-fold for **1a**, 50-fold for **1b**) to observe M−H···N bond formation (Figure 3, see also Figure S2). On the other hand, more basic properties of the N-bases (higher pK_a of conjugated acids, Table 1) in comparison with phosphine oxides allow easy proton transfer, and therefore it was difficult to stop the process at the hydrogen-bond formation step. Thus, we showed hydrogen bonding with Py but could not quantitatively characterize these bonds. In the case of even more basic NEt_3, we could not detect hydrogen-bonded complexes, because proton transfer readily occurs with this base due to an even lower proton transfer barrier (see theoretical part below).

2. Proton Transfer. 2.1. Interaction between 1 and Bases in Nonpolar Medium. The spectral evidence of hydrogen-bond formation between **1b** and Py was obtained at large base excess (50-fold). At twice larger concentration of Py (1:100), the proton transfer takes place at a very low temperature of only -190 K. At that the acidity increase on going to molybdenum analogue **1a** induces partial proton transfer at substantially smaller Py excess: deprotonation takes place at 1:10 and even 1:5 **1a**:Py ratios when the MH···N complex is scarcely visible (Figure 3). Under these conditions, the broad low frequency bands (1890 and 1770 cm^{-1}) were observed, being assigned to the ion pairs **3a**.[53] Their intensity increases in time (during one-half an hour); however, precipitation of the ionic product precluded obtaining the reliable kinetic data.

In the presence of a 10-fold HMPA excess, the ν_{CO} bands of ionic forms **3**[53] appear at 1894, 1776 cm^{-1} for molybdenum and 1890, 1772 cm^{-1} for tungsten at 210 and 200 K, respectively. Upon cooling to 190 K, the ν_{CO} shoulders of hydrogen-bonded complexes decrease, and the intensity of new bands grows reversibly (Figure S3). Thus, at low temperatures, three forms are present in equilibrium: initial hydride **1**, hydrogen bonded-intermediate **2**, and ion pair **3** (Scheme 1).

Proton transfer equilibrium constants, K_{1-3}, were determined from the intensity changes of the ν_{CO}(**3**) bands as the sum of hydrogen bonding (**1**↔**2**) and proton transfer (**2**↔**3**) steps: $K_{1-3} = K_{1-2} \cdot K_{2-3} = [\mathbf{3}]/(c_\mathbf{1} - [\mathbf{3}])(c_{HMPA} - [\mathbf{3}])$. Thermodynamic parameters of proton transfer were determined from the temperature dependence of ln K_{1-3} in the 180−220 K range (see plots in Figure S5): for **1a** $\Delta H°_{1-3} = -9.7 \pm 0.9$ kcal mol^{-1}, $\Delta S°_{1-3} = -35 \pm 5$ eu, and for **1b** $\Delta H°_{1-3} = -7.8 \pm 0.3$ kcal mol^{-1}, $\Delta S°_{1-3} = -30 \pm 1$ eu. Subtraction of the corresponding values for the hydrogen-bonding step reported above gives parameters of the proton transfer stage: $\Delta H°_{2-3} = -6.5$ kcal mol^{-1}, $\Delta S°_{2-3} = -25$ eu for **1a** and $\Delta H°_{2-3} = -5.3$ kcal mol^{-1}, $\Delta S°_{2-3} = -25$ eu for **1b**. These data allow one to present the energy profile for the reaction between the hydrides and HMPA (Figure 4).

The first energy minimum belongs to the hydrogen-bonded complex MH···B, and the second one belongs to the ion pair M^-···$^+$HB stabilized by a hydrogen bond between the organic cation and the organometallic anion. The first minimum is deeper for molybdenum than for tungsten hydride in accordance with the stronger H-bond of the former. Proton transfer for this hydride is also thermodynamically more preferred, and thus the second minimum is also deeper for **1a**, correlating with greater acidity (pK_a) of this hydride in comparison with **1b**. The activation barriers were not experimentally determined and will be discussed in the theoretical section (see below).

2.2. Quantum Chemical Study of Hydrogen Bonding and Proton Transfer in the Gas Phase. Describing the $CpM(CO)_3H$···B interaction for the first time,[6] we reported also the results of DFT/B3LYP calculations of hydrogen-bonded complexes with pyridine. Herein, we report the results of DFT optimization of adducts with pyridine, trimethylamine, and trimethylphosphine oxide at the M05 theory level. This new functional was introduced recently to describe better, among other problems, intermolecular interactions for transition metal complexes.[54] The new results obtained for hydrogen-bond formation energies, geometrical and electronic characteristics,

(51) Matrosov, E. I.; Tsvetkov, E. N.; Lobanov, D. I.; Malevannaya, R. A.; Kabachnik, M. I. *J. Gen. Chem.* **1972**, *42*, 1218.
(52) Matrosov, E. I.; Tsvetkov, E. N.; Malevannaya, R. A.; Kabachnik, M. I. *J. Gen. Chem.* **1972**, *42*, 1695.
(53) Darensbourg, M. Y. *Prog. Inorg. Chem.* **1985**, *33*, 221–274.

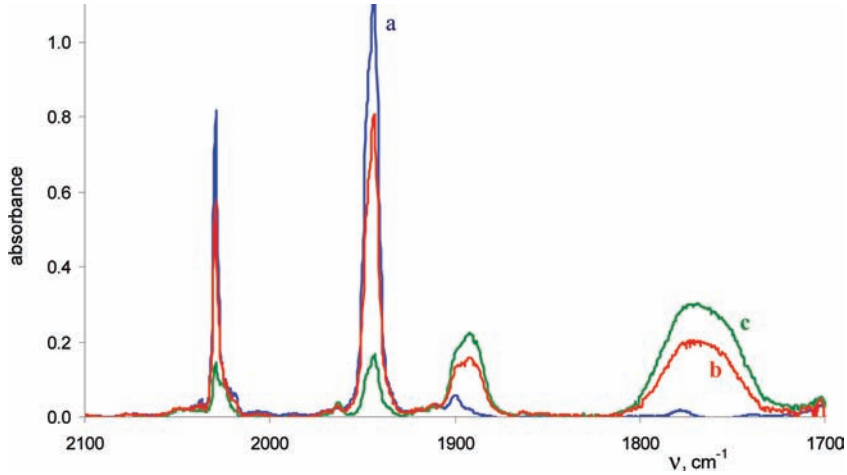

Figure 3. IR spectra in the ν_{CO} range of $CpMo(CO)_3H$ (0.001 M (a)) in excess Py ((b) 0.005 M, (c) 0.01 M). Hexane, 190 K.

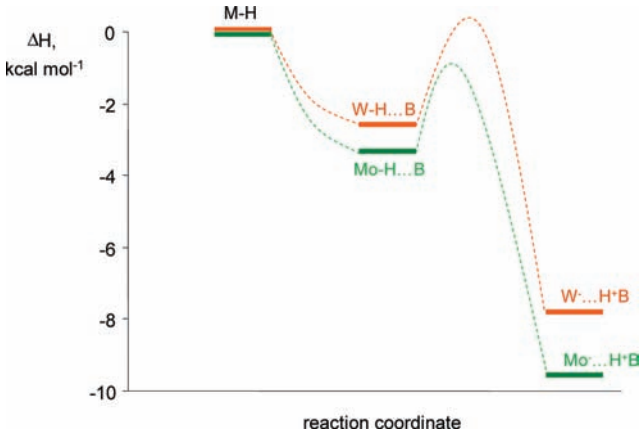

Figure 4. Energy profile ($\Delta H°$) for the proton transfer reaction between hydrides **1a** and **1b** and HMPA in hexane.

as well as the ν_{CO} and ν_{MH} stretching vibration frequencies are gathered in Table 3; the calculated geometries are shown in Figure 5.

The calculated formation energies of the hydrogen-bonded complexes (ΔE_{ZPVE}) span the range between −3.8 and −4.8 kcal mol^{-1}. Taking into account the basis set superposition error, these numbers diminish to −1.6 to −2.6 kcal mol^{-1}. These values are comparable to the energies reported for some CH···Y bonds, but are notably lower than the interaction energies of Cl_3CH or CF_3CH with Py.[55−58]

The (M)H···N distances in the complexes calculated (Table 3) are reasonably short and comparable to the CH···N contacts in hydrogen-bonded complexes of similar strength.[55,57] The practically linear arrangement of the hydrogen-bonded moiety with M−H···N angles over 170° is not a surprise because linearity is a common feature of intermolecular classical and nonclassical hydrogen bonds.[2,3,59] A deviation from linearity is probably caused by additional interactions between the CH-groups of bases and the carbonyl groups of the hydride as evidenced by rather short C−H···O(C) distances (2.65−2.91 Å) (see below). Hydrogen bonding leads to electronic redistribution in both interacting molecules. The negative charge of the nitrogen atom in the MH···N hydrogen bond increases similarly to the classical XH···N bond.[60] Positive charge on the metal bound hydrogen atoms increases by 0.053−0.084 units. The M−H bond polarization is similar to that of, for example, CF_3H[56] and, as expected, increases upon hydrogen-bond formation (Table 3). Although there is a very limited number of data available for C−H proton donors with the same bases, comparison of the complexes formed by **1** and nitrogen bases (Py, Me_3N) with those of Hal_3CH (Hal = F,[56] Cl[58]) with Py and NH_3 shows that X−H bond polarization increases similarly for both types of proton donors. However, in the case of M−H···N bonds, this polarization occurs at substantially lower interaction energy (Figure S7) and at notably lower electron density (charge) transfer from the lone pair of the base n(Y) to σ^*(M−H) (Figure 6). The latter is responsible for these changes making a major contribution to the interaction energy as for any hydrogen bond (Table 3).[61]

"Atoms in molecules" analysis[62,63] reveals (3,−1) critical points between "hydride" and electronegative atom of base (X = N or O), which are indicative of hydrogen-bond formation. The energies of M−H···X bonds obtained by AIM approach (Table 4) are very close to ΔE_{BSSE} and to the experimental hydrogen-bonding enthalpy values.

Additional contacts (hydrogen bonds) between CH groups of bases and carbonyl ligands of **1** are found for each hydrogen-bonded complex calculated (Figure 7). The energy of each of these CH···O(C) interactions estimated under AIM approach is lower than the energy of the M−H···X hydrogen bond (Table 4), but their net impact to the total complexation energy is ca. 50% (compare ΔE_{ZPVE} (Table 3) and E_{cont} (Table 4)). The bond ellipticity ε values (0.01−0.07) indicate cylindrical (linear) bond path between the metal bound hydrogen and the basic nitrogen/oxygen. In the case of pyridine and phosphine oxide adducts, the forced CH···O contacts possess nonlinear bond paths ($\varepsilon \approx$

(54) Zhao, Y.; Schultz, N. E.; Truhlar, D. G. *J. Chem. Theory Comput.* **2006**, *2*, 364–382.
(55) Gu, Y.; Kar, T.; Scheiner, S. *J. Mol. Struct.* **2000**, *552*, 17–31.
(56) Alabugin, I. V.; Manoharan, M.; Peabody, S.; Weinhold, F. *J. Am. Chem. Soc.* **2003**, *125*, 5973–5987.
(57) Domagala, M.; Grabowski, S. J. *Chem. Phys.* **2009**, *367*, 1–6.
(58) Li, A. Y.; Wang, S. W. *J. Mol. Struct. (THEOCHEM)* **2007**, *807*, 191–199.
(59) Jeffrey, G. A. *An Introduction to Hydrogen Bonding*; Oxford University Press: New York, 1997.
(60) Scheiner, S. *Hydrogen Bonding. A Theoretical Perspective*; Oxford University Press: New York, 1997.
(61) Rauk, A. *Orbital Interaction Theory of Organic Chemistry*, 2nd ed.; John Wiley & Sons, Inc.: New York, 2001; pp 137−149.
(62) Bader, R. F. W. *Atoms in Molecule, a Quantum Theory*; Clarendon Press: Oxford, U.K., 1990.
(63) Bader, R. F. W. *Chem. Rev.* **1991**, *91*, 893–928.

Table 3. Selected Structural, Electronic, and Spectroscopic Parameters Calculated for Free Hydrides **1** and Their Hydrogen-Bonded Complexes with Bases

	1a	**1a**/Py	**1a**/Me_3N	**1a**/Me_3PO	**1b**	**1b**/Py	**1b**/Me_3N	**1b**/Me_3PO
ΔE_{ZPVE}, kcal mol^{-1}		−4.5	−4.8	−6.9		−3.9	−4.6	−7.0
ΔE_{BSSE}, kcal mol^{-1}		−2.1	−2.6	−4.1		−1.7	−2.2	−3.9
$E_{n\rightarrow\sigma^*}$,[a] kcal mol^{-1}		1.65	2.65	2.35, 1.45[b]		1.17	1.56	2.12, 1.47[b]
r(M−H), Å	1.713	1.715	1.725	1.717	1.725	1.723	1.730	1.723
r(H···Y[c]), Å		2.476	2.329	2.139		2.506	2.431	2.156
∠MH···Y,[c] deg		171.0	177.7	172.3		165.7	170.2	171.7
Δq(M)[d]		0.055	0.051	0.057		0.037	0.036	0.042
Δq(H)[d]		0.053	0.053	0.076		0.059	0.058	0.084
Δq(Y[c])[d]		−0.023	−0.006	−0.012		−0.024	−0.008	−0.013
M−H polarization[e]	40.5	36.5	36.1	36.9	42.1	40.0	39.3	37.8
ν_{M-H},[f] cm^{-1}	1812	1825 (+13)	1756 (−56)	1830 (+17)	1893	1915 (+22)	1845 (−48)	1903 (+10)
A_{M-H},[g] 10^4 L mol^{-1} cm^{-2}	0.23	0.92	2.45	1.76	0.12	0.97	1.46	1.93
ν^1_{CO} (s, A′),[f] cm^{-1}	2117	2102 (−15)	2101 (−16)	2097 (−20)	2117	2102 (−14)	2101 (−15)	2097 (−20)
ν^2_{CO} (as, A″),[f] cm^{-1}	2048	2029 (−19)	2029 (−19)	2026 (−22)	2043	2028 (−15)	2027 (−16)	2022 (−21)
ν^3_{CO} (as, A′),[f] cm^{-1}	2045	2020 (−25)	2015 (−30)	2003 (−42)	2042	2019 (−23)	2015 (−28)	2002 (−40)

[a] Energy of donation from the lone pair of the base (n(Y)) to σ^*(M−H). [b] Interaction of hydride with each of two oxygen lone pairs. [c] Y = O or N. [d] Change of the NBO charge at the given atom. [e] Electron density at the metal bound hydrogen relative to the total electron density on σ(M−H), in %. [f] Frequency shift ($\Delta\nu$) relative to the isolated **1** is given in parentheses, $\Delta\nu = \nu$(complex) − ν(**1**). [g] Calculated intensity of M−H vibration.

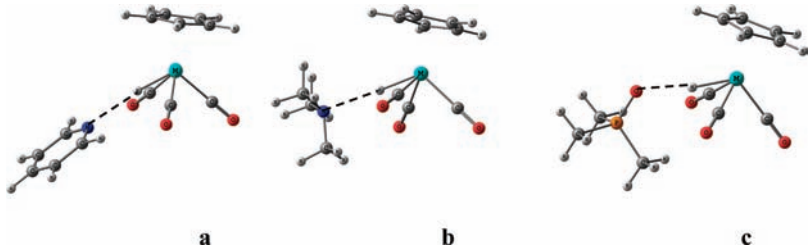

Figure 5. The calculated geometry of hydrogen-bonded complexes between $CpM(CO)_3H$ and Py (a), $N(CH_3)_3$ (b), and Me_3PO (c).

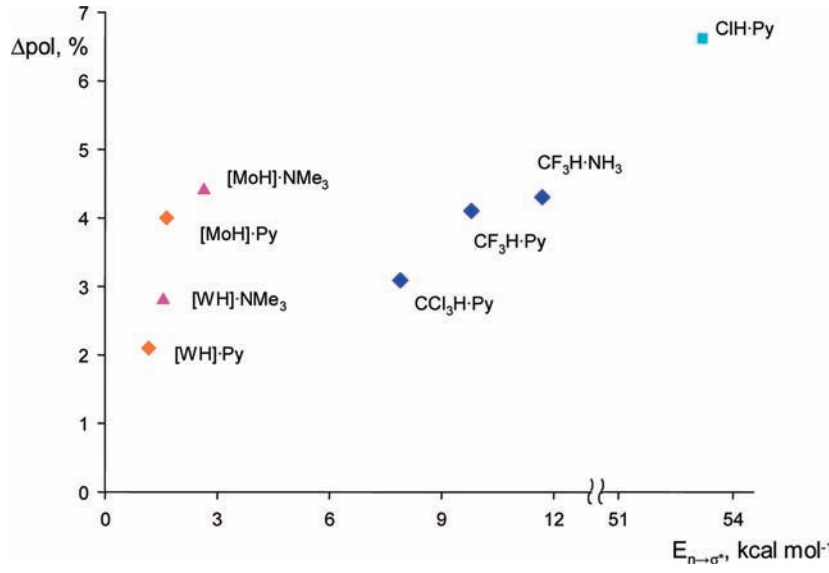

Figure 6. Dependence of the X−H (X = C, Mo, W) bond polarization change (Δpol, in % on H) on the energy of n(Y) to σ^*(M−H) donation ($\Delta E_{n\rightarrow\sigma^*}$) for hydrides **1** or halomethanes (CF_3H,[56] CCl_3H[58]) interacting with nitrogen bases. Point for ClH·Py complex is shown for the sake of comparison with classical highly polarized proton donor.

up to 0.12−0.14), whereas these contacts are not so restrained in amine adducts due to the methyl groups flexibility ($\varepsilon \approx$ 0.03−0.07).

The presence of these multiple interactions of comparable energy can be recalled as a likely cause of the calculated changes in geometrical and spectral parameters upon hydrogen-bonded complexes formation. The general trend observed for organic systems is that the X−H bond elongates upon hydrogen-bond formation, and this causes the red shift of ν_{XH} band and its intensity increase.[56,59] The C−H bond often contracts upon hydrogen-bond formation, which causes the blue shift of ν_{CH} band and its intensity decrease.[55−57,64,65] As expected, the M−H bonds' elongation by 0.002−0.012 Å is found except for the **1b**·Py and **1b**·$OPMe_3$ complexes, where the W−H bond shortens by 0.002 Å. Molybdenum hydride complexes with Py

(64) Joseph, J.; Jemmis, E. D. *J. Am. Chem. Soc.* **2007**, *129*, 4620–4632.
(65) Wojtulewski, S.; Grabowski, S. J. *Chem. Phys.* **2005**, *309*, 183–188.

Table 4. AIM Parameters of the Hydrogen-Bonded Complexes between Hydrides **1** and Bases

	1a/Py		**1a**/Me_3N		**1a**/Me_3PO		**1b**/Py		**1b**/Me_3N		**1b**/Me_3PO	
	MoH···N	CH···O(C)[a]	MoH···N	CH···O(C)[b]	MoH···O	CH···O(C)[c]	WH···N	CH···O(C)[a]	WH···N	CH···O(C)[b]	WH···O	CH···O(C)[c]
r(H···X),[d] Å	2.476	2.668−2.691	2.329	2.772−2.905	2.139	2.662−2.794	2.506	2.722−2.733	2.431	2.789−2.793	2.156	2.651−2.787
ρ_c[e]	0.013	0.006−0.006	0.018	0.005−0.004	0.020	0.006−0.005	0.012	0.005−0.005	0.015	0.005−0.005	0.019	0.006−0.005
$\nabla^2\rho_c$[f]	−0.007	−0.006 to −0.005	−0.009	−0.005 to −0.004	−0.013	−0.005 to −0.005	−0.007	−0.005 to −0.005	−0.008	−0.005 to −0.004	−0.013	−0.005 to −0.005
ε[g]	0.010	0.090−0.102	0.032	0.061−0.029	0.072	0.036−0.108	0.016	0.129−0.139	0.026	0.072−0.025	0.067	0.083−0.118
E_{con}, kcal mol^{-1}	−2.1	−1.2 to −1.1	−2.9	−0.9 to −0.7	−3.8	−1.1 to −0.9	−2.1	−1.0	−2.5	−0.9	−3.7	−1.2to −0.9

[a] Two contacts. [b] Four contacts. [c] Three contacts. [d] X = N or O of the base or O of the carbonyl ligand. [e] ρ_c: electron density at the (3,−1) bond critical point. [f] Laplacian of the electron density at the bond critical point. [g] Hydrogen-bond ellipticity defined as $\varepsilon = (\lambda_1/\lambda_2 - 1)$, where λ_1 and λ_2 are the negative eigenvalues of the Hessian of the electron density at the bond critical point ordered such that $\lambda_1 < \lambda_2 < 0$.

Figure 7. Molecular graphs of hydrogen-bonded complexes of $CpWH(CO)_3$ with Me_3N (a), Py (b), and Me_3PO (c). Color codes: small red, bond critical points; small yellow, ring points; small green, cage points; black, carbon atoms; blue, nitrogen atoms; red, oxygen atoms; brown, phosphorus atoms; gray, hydrogen atoms; and white, tungsten atom.

and $OPMe_3$ feature the ν_{MH} blue shift despite the M−H bond elongation and band intensity increase, whereas tungsten hydride complexes with the same bases feature the M−H bond contraction and blue shift accompanied by the band intensity increase. Such changes are counterintuitive but could be caused by the above-mentioned simultaneous CH···O(C) and M−H···X interactions. CH···O(C) interaction should lead to M−H bond contraction and blue shift in contrast to M−H bond elongation and concomitant red shift caused by M−H···X interaction. Being superimposed, these two effects of comparable energy lead to the abnormal changes calculated. CH···O(C) contacts are weakest in **1**·NMe_3 complexes, which conform the general spectral trend (Table 3). In solution, the carbonyl groups of **1** are apparently blocked by the CH···O(C) interaction with solvent molecules. This prevents CH···O(C) bonding with the CH groups of the bases. Consequently, the M−H···X hydrogen-bond formation dominates in hydride−base interaction and determines the spectroscopic changes observed (the red shift of the ν_{MH} bands).

Formation of the MH···B hydrogen bond entails the lower frequency ν_{CO} band shift (Table 3). Different values of the shift for $\nu_{CO}{}^2$ and $\nu_{CO}{}^3$ lead to the partition of these two bands by 9−23 cm^{-1} in comparison to 1−3 cm^{-1} in the isolated hydrides. However, these results should be handled with caution because they are obtained for complexes in the gas phase. Smaller band shift and thus lower band separation are expected in solution. Indeed, one broad $\nu_{CO}{}^{as}$ band is observed experimentally in the presence of bases at the frequencies lower than in the starting hydrides being an envelope of two vibrations.

Proton transfer from MH to the nitrogen of the base goes along the linear M−H−N hydrogen bond, yielding the $[M]^-\cdots[HN]^+$ ion pair as the reaction product. This process does not involve a significant structural reorganization of the $CpM(CO)_3$ moiety. Concomitant electronic reorganization involves electron density shift from carbonyl ligands to the core metal as reflected by the ν_{CO} frequency shift. Proton transfer transition states feature the N···H distances in the range

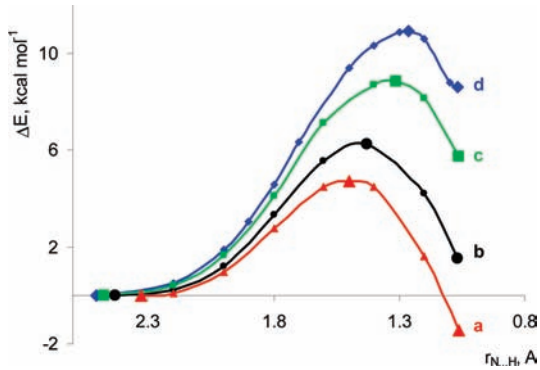

Figure 8. Energy profiles calculated for proton transfer from hydrides **1** to N-bases: $CpMo(CO)_3H/Me_3N$ (a), $CpW(CO)_3H/Me_3N$ (b), $CpMo(CO)_3H$/Py (c), and $CpW(CO)_3H$/Py (d). Energies of hydrogen-bonded complexes are taken as zero of energies. Enlarged symbols correspond to the optimized minima and transition states.

1.262−1.501 Å. In agreement with Hammond's postulate,[66] longer NH distances in the transition state are found for stronger hydrogen-bonded complexes, indicating easier deprotonation of the metal hydride. The energetic diagram of proton transfer taking the N−H distance as the reaction coordinate (Figure 8) demonstrates rather low activation barrier. In three of the four complexes, the ionic form is less preferable than hydrogen-bonded complexes in the gas phase. Only the strongest **1a**·NMe_3 system forms an energetically favorable ion pair.

An interesting point to discuss is the structure of the hydrogen-bonded ion pair. So far, we considered only ionic complexes of one type formed as the immediate result of proton transfer from **1** to base. This ion pair (**A**, Figure 9) is stabilized by the $NH^+\cdots M^-$ hydrogen bond. However, two more possibilities[53] exist as depicted in Figure 9. The ion pair **B** with a hydrogen bond to one of the CO-groups ($NH^+\cdots OC$) features the most substantial distortion of the $M(CO)_3$ moiety; this ion pair was found for pyridinium cation only. The ion pair **C** features a hydrogen bond to the metal atom as well, but the cation approaches from the side opposite to the Cp ring, and could be envisaged as the result of dissociation−reassociation of the ionic proton transfer product **A**. The calculated energies, main structural parameters, and spectroscopic characteristics (ν_{CO} frequencies and intensities) of these ion pairs are collected in Table 5. The interaction with Me_3NH^+ does not perturb the anion symmetry in **C** as is evident from similar values of the $\nu_{CO}{}^2$ and $\nu_{CO}{}^3$ frequencies. In the case of PyH^+, there is some symmetry perturbation, but the difference between the $\nu_{CO}{}^2$ and $\nu_{CO}{}^3$ frequencies in **C** is much less than in other two isomers. The linearity of the hydrogen bond is maximal in complexes with trimethylammonium $[Me_3NH]^+\cdots[M]^-$ ($\angle M\cdots HN$ = 176−180°); in complexes with pyridinium the $NH\cdots X$ angles are 171−173°. Configuration **C** is energetically most favorable, and we suppose that the ion pairs observed in the experiment are of this type.

2.3. Solvent Effects. The solvents chosen for the spectroscopic study, hexane, dichloromethane (DCM), THF, and acetonitrile (AN), differ in polarity (determined here as dielectric permittivity) and in hydrogen-bonding ability (Table 6). Their low melting point allows IR study at low temperatures (down to 190−230 K). Table 7 shows variation of spectroscopic characteristics of the ν_{CO} bands of $CpM(CO)_3H$ hydrides with solvent

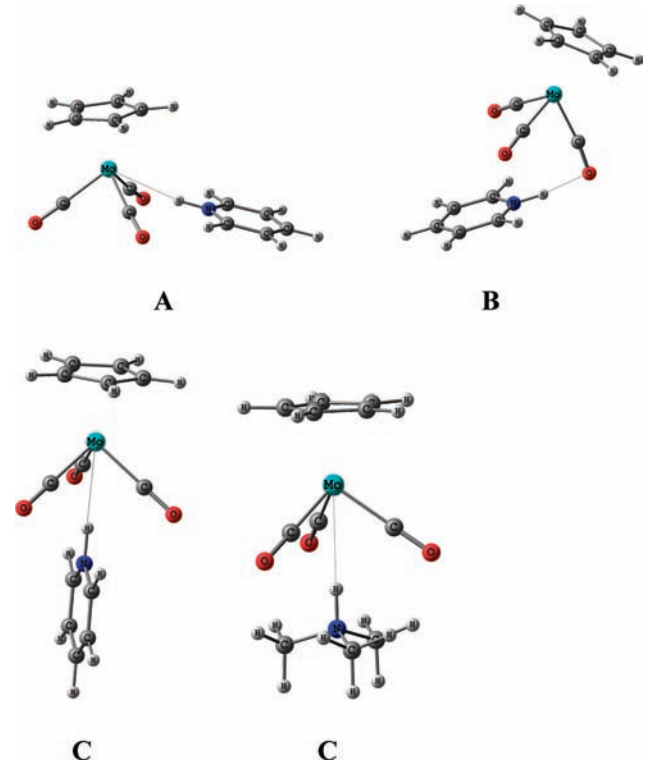

Figure 9. Three types of hydrogen-bonded ion pairs between $CpM(CO)_3^-$ anion and protonated bases on the example of PyH^+ and Me_3NH^+.

at low temperatures. As one can see, the low frequency shift (by 7−18 cm^{-1}) and broadening of ν_{CO} bands occur upon transition from "inert" hexane to other solvents. Note that there is no dependence of the ν_{CO} band position on solvent (THF, DCM, AN), but the broadening of the $\nu_{CO}{}^{as}$ band increases in the order: hexane ≪ THF < AN < DCM (Figure 10). The molar extinction coefficient in the band maxima decreases considerably in the order: hexane ≫ THF > AN ≈ DCM. This sequence correlates with the solvent hydrogen-bonding ability. Maximal half-height full width ($\Delta\nu_{1/2}$) of the $\nu_{CO}{}^{as}$ band is observed in DCM, which could form $CH\cdots OC$ hydrogen bonds with carbonyl ligands of **1**. Surprisingly, although THF and AN are rather strong hydrogen-bond acceptors, the sequence of the $\Delta\nu_{1/2}{}^{as}$ changes does not correspond to the solvents E_j[26] or β[17,67] factors but to the order of their proton-donating ability α[17,67] (Table 6). Computations support this possibility showing $CH\cdots OC$ interactions between **1b** and AN, THF, DCM with the energies 2.3−1.5 kcal mol^{-1} comparable to that of $MH\cdots$base hydrogen bonds (see the Supporting Information for details).

At that, being a rather strong proton acceptor in hydrogen bond (E_j = 1.04),[26] THF interacts with hydrides **1** yielding $M-H\cdots O$ hydrogen-bonded complexes. The appearance of new low-frequency ν_{CO} shoulders was observed upon addition of a 100-fold excess of THF to the hydrides **1** in hexane at 190 K (Figure 11) as in the presence of phosphine oxides. The formation enthalpy, $\Delta H_{1-2}°$, for complexes of **1a** and **1b** with THF in hexane was estimated using the "rule of factors"[26] as −2.6 and −2.1 kcal mol^{-1} for **1a** and **1b**, respectively. These values are close to the formation enthalpy for complexes with HMPA.

(66) Bruckner, R. *Advanced Organic Chemistry: Reaction Mechanisms*; Harcourt/Academic Press: San Diego, CA, 2002; p 636.
(67) Cook, J. L.; Hunter, C. A.; Low, C. M. R.; Perez-Velasco, A.; Vinter, J. G. *Angew. Chem., Int. Ed.* **2007**, *46*, 3706–3709.
(68) Reichardt, C. *Solvents and Solvent Effects in Organic Chemistry*, 3rd ed.; Wiley-VCH: Weinheim, 2003; p 653.

Table 5. Calculated Gas-Phase Formation Energies (in kcal mol^{-1}), Main Spectroscopic (ν_{CO} Frequency, in cm^{-1}, and Intensity A_{CO}, in 10^4 L mol^{-1} cm^{-2}), and Structural (Distances in Å, Angles in deg) Parameters of Hydrogen-Bonded Ion Pairs between Anions **3** and Protonated Bases

	3a/PyH$^+$			**3b**/PyH$^+$			**3a**/Me$_3$NH$^+$		**3b**/Me$_3$NH$^+$	
	A	**B**	**C**	**A**	**B**	**C**	**A**	**C**	**A**	**C**
ΔE_{zpe}[a]	+5.2	+5.4	+3.5	+8.0	+7.8	+5.6	−1.3	−4.9	+1.6	−3.0
ν_{CO}^1	2029	1972	1988	2026	1972	1989	2032	1980	2029	1980
ν_{CO}^2	1913	1892	1909	1910	1893	1912	1917	1882	1915	1884
ν_{CO}^3	1871	1791	1888	1871	1797	1890	1870	1881	1870	1883
A_{CO}^1	10.03	5.21	3.30	10.45	5.35	3.48	9.14	5.38	9.58	5.52
A_{CO}^2	7.25	9.31	11.50	7.25	9.51	11.73	8.13	10.67	8.22	10.86
A_{CO}^3	11.23	9.33	10.88	11.47	9.58	10.99	10.84	10.63	11.14	10.74
*r*X···H	2.605[b]	1.728[c]	2.636[b]	2.616[b]	1.729[c]	2.625[b]	2.604[b]	2.737[b]	2.615[b]	2.722[b]
*r*N−H	1.065	1.037	1.052	1.067	1.037	1.055	1.064	1.047	1.067	1.048
∠X···HN	171[b]	172[c]	173[b]	173[b]	172[c]	173[b]	176[b]	180[b]	178[b]	180[b]

[a] Relative to the energy of the separated neutral reactants (**1**, base) energies. [b] X = M. [c] X = O(C).

Table 6. Properties of the Solvents Used

	T_{melt}, K	E/P_i[a] [26]	β/α[b] [17]	ε,[c] 298 K [68]	ε[c] (*T*, K)
hexane (heptane)	178		0.3/0.4	1.89 (1.92)	
THF	165	1.04/−	5.3[d]/0.9[d]	7.58	12.50 (190)[23,24]
DCM	178	−/0.25	1.1/1.9	8.93	15.53 (190)[22]
AN	227	0.75/−	4.7/1.7	35.94	47.56 (230)[25]

[a] Basicity (E_j)/acidity (P_i) factors. [b] Hydrogen-bond acceptor (β)/donor (α) parameters. [c] ε: dielectric permittivity. [d] Data for alkyl ether.

The proton-donating ability of DCM (P_i = 0.25[26]) is only slightly less than that of hydrides **1** (P_i are equal 0.35 and 0.44 for **1b** and **1a**, respectively). Thus, DCM could interact as a proton donor with chosen bases. For example, variable temperature study of interaction between HMPA with 5-fold excess of DCM in hexane (ν_{PO} band changes, see Figure S6) gives $\Delta H° = -2.1 \pm 0.2$ kcal mol^{-1}, $\Delta S° = -3.9 \pm 0.8$ eu. The obtained enthalpy is comparable to that of complexes between HMPA and **1**. Still at 290 K in DCM, when proton transfer occurs at lower extent, the low frequency shoulder on the ν_{CO}^{as}(**1**) band is observed in the presence of Et$_3$N, evidencing the MH···NEt$_3$ bond formation. Under these conditions, the bands of both **1a** and **1b** broaden by 4 cm^{-1}.

2.3.1. Solvent Effect on Proton Transfer: Quantum Chemical Calculations. The energies of the molecular and ionic H-complexes as well as of the transition states for proton transfer in different solvents were calculated under the single-point CPCM approach.[34,35] The ion pair type **C** was considered as the final proton transfer product. The data obtained are collected in Table 8; Figure 12 illustrates graphically the trends revealed at the example of the CpMo(CO)$_3$H/Py system.

Perusal of the data obtained shows that the minima of molecular H-complexes become shallower, ΔE_{HB} dropping significantly (by ca. 4 kcal mol^{-1}) from the gas phase to solution and varying within less than 1 kcal mol^{-1} with the solvent. The second minima belonging to the ion pairs become deeper in more polar environment, the ion pair formation becoming more energetically favorable in the order heptane < THF ≈ DCM < AN. The calculated barriers of proton transfer (designated here as the activation energy $\Delta E_a = E_{TS} - E_{HB}$) decrease slightly (<2 kcal mol^{-1}) on going from the gas phase to solution and with solvent polarity, reaching the minimum value in the most polar solvent acetonitrile in accord with the ionic character of TS. The same influence of the solvent polarity in the proton transfer barrier was found when hydride is playing the role of proton acceptor.[69] According to CPCM calculations, proton transfer in this solvent could be observed from both **1a** and **1b** to either Py or Me$_3$N. Low barriers of proton transfer to Me$_3$N (<5 kcal mol^{-1}) and high ion pair stabilization energy (8−13 kcal mol^{-1}) evidence easy reaction in all media. For pyridine, the result of the interaction depends on the partner hydride and

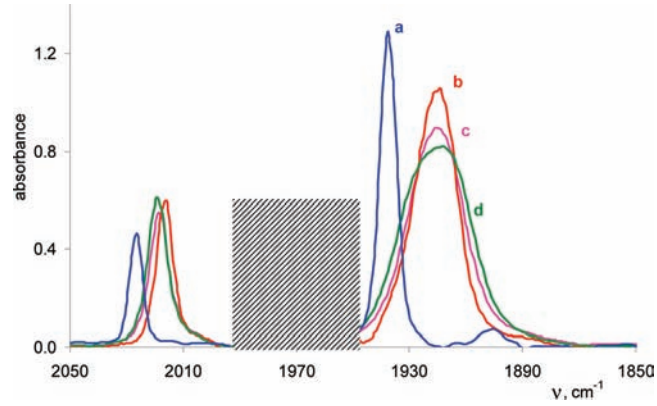

Figure 10. IR spectra in the range ν_{CO} of CpW(CO)$_3$H in hexane (0.0005 M) (a), in THF (0.002 M) (b), in AN (0.002 M) (c), and in DCM (0.002 M) (d). l = 0.12 cm. Shaded area denotes the region masked by the THF absorption.

Table 7. Spectroscopic Characteristics of CpM(CO)$_3$H Hydrides in Different Solvents at Low Temperatures

hydride	solvent[a]	ν^sCO[b]	$\Delta\nu_{1/2}^s$ [c]	ε_{CO}[d] ×10^{-3}	A ×10^{-4} (230 K)[e]	ν^{as} [b]	$\Delta\nu_{1/2}^{as}$ [c]	ε_{CO}[d] ×10^{-3}	A ×10^{-4} (230 K)[e]
1a	hexane (190)	2029	5.5			1944	8		
	THF (190)	2020	7.5	3.0	2.7 ± 0.1	1929	21	4.5	9.6 ± 0.6
	DCM (190)	2022	9	2.3 ± 0.2	2.4 ± 0.3	1928	31	2.9 ± 0.2	8.7 ± 1.2
	AN (230)	2022	9	1.4	2.5 ± 0.3	1929	24	2.1	9.8 ± 1.4
1b	hexane (190)	2026	5			1936	8		
	THF (190)	2016	7	2.9 ± 0.2	2.0 ± 0.2	1920	18	5.0 ± 0.3	8.5 ± 0.3
	DCM (190)	2018	8.5	2.7 ± 0.2	2.7 ± 0.3	1918	30	3.6 ± 0.2	10.0 ± 0.7
	AN (230)	2019	8	2.4 ± 0.1	2.5 ± 0.1	1920	23	3.9 ± 0.2	10.2 ± 0.4

[a] In parentheses is shown the lowest temperature (in K) possible for IR measurements in the given solvent. All of the data are obtained at this temperature. [b] In cm^{-1}. [c] Half-height full widths $\Delta\nu_{1/2}$ in cm^{-1}. [d] Molar extinction coefficients ε_{CO} in L mol^{-1} cm^{-1}. [e] Integral intensity in L mol^{-1} cm^{-2}.

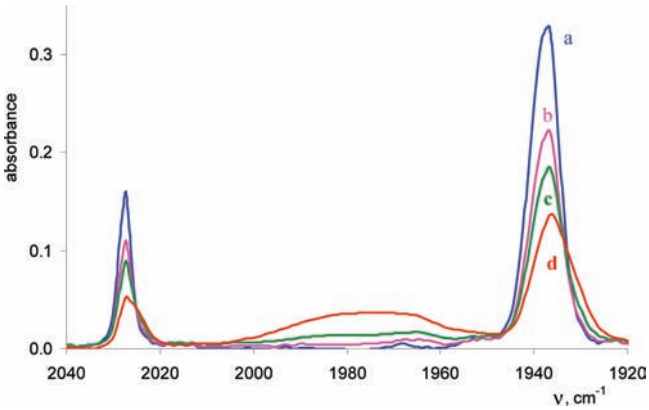

Figure 11. IR spectra (ν_{CO} range) of $CpWH(CO)_3$ (0.0005 M (a)) in the presence of THF (0.05 M (b), 0.15 M (c), 0.45 M (d)). Hexane, 190 K. l = 0.12 cm. Broad band between 2000−1950 cm^{-1} is due to THF absorption.

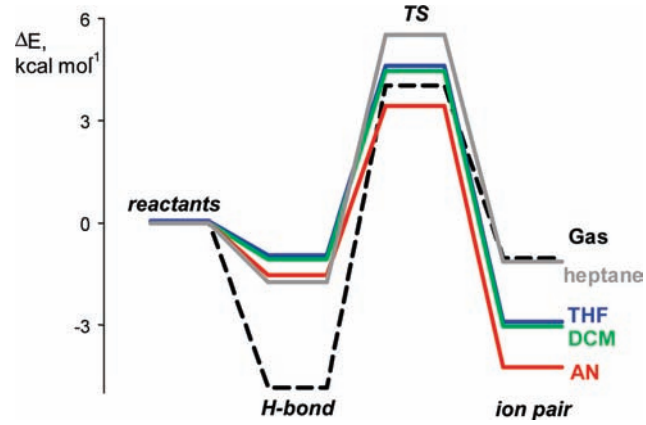

Figure 12. Calculated energy profile of proton transfer from $CpMo(CO)_3H$ to Py in the gas phase and different media.

solvent. For hydride **1a**, deprotonation by pyridine is thermodynamically feasible in all solvents, but the reaction is endothermic in heptane. For the **1b**/Py system, featuring the weakest interaction, the highest reaction barriers and least favored ion pair formation are found. The computation predicts the proton transfer to be spontaneous only in acetonitrile; in other less polar solvents, the ion pair formation energy is slightly positive.

2.3.2. Solvent Effect on Proton Transfer: Experimental Study. Dissociation of the Mo−H bond of **1a** is observed as the result of its dissolution in acetonitrile at 230 K. The process is a rather slow, gradual intensity decrease of ν_{CO} bands of **1a** (2022 and 1929 cm^{-1}), and the appearance of two lower-frequency ν_{CO} bands of **3a** (1896 and 1776 cm^{-1}) is observed in time. The reaction rate constant was obtained by monitoring the ν_{CO}(**1a**) bands decrease, $k = 3.45 \pm 0.05 \times 10^{-5}$ s^{-1}, $\Delta G_{230K}^{\ddagger} = 18.0$ kcal mol^{-1}. Tungsten hydride **1b** is stable in acetonitrile; no solvolysis was observed. Similar phenomenon was observed when both complexes **1** are dissolved in neat pyridine ($\varepsilon = 12.3$[68]). The proton transfer occurs even at room temperature, and it is quantitative in the case of **1a**: only the ν_{CO} bands of the anion are observed (1895 and 1776 cm^{-1}). In the case of **1b**, the ν_{CO} bands of the anion (1888 and 1770 cm^{-1}) reversibly grow up with temperature decrease. Quantitative analysis of the intensity changes gave thermodynamic parameters for the proton transfer step for tungsten hydride: $\Delta H_{2-3}^{\circ} = -7.0 \pm 0.5$ kcal mol^{-1}, $\Delta S_{2-3}^{\circ} = -26.0 \pm 1.7$ eu.[6] The reaction is fast at all temperatures in pyridine in agreement with stronger bonding and thus lower barrier with this base.

Proton transfer to a very strong base NEt_3 is quantitative in acetonitrile at 230 K as in other solvents. The interaction between **1** and HMPA or pyridine in acetonitrile at 230 K is immediate and leads to partial proton transfer. In the case of more acidic **1a**, the 10-fold excess of both bases is enough to get the extent of proton transfer (determined as the ratio of equilibrium concentration of **1** to its total concentration) about 20% for HMPA and 60% for pyridine. For **1b**, the proton transfer occurs at a much lower extent even at higher base excess (50-fold in the case of HMPA and 10-fold for pyridine give 8% and 5% of proton transfer, respectively). Similar semiquantitative trends were found in other solvents, DCM and THF, but the proton transfer extent appears to be substantially lower in these medium polarity solvents than in polar AN or nonpolar hexane. This necessitates the use of much higher base excess.

To get quantitative data, the equilibrium constants of proton transfer reaction were determined as $K_{1-3} = [M^{-}\cdots{}^{+}HB]/([MH]^*[B])$ using intensity changes of ν_{CO} bands of **1**, and the reaction free energies, ΔG_{1-3}, were calculated (Table 9). In agreement with the above description, the K_{1-3} values at 230 K are higher in AN in comparison to hexane. In the case of medium polarity solvents, the values of K_{1-3} occurred to be appreciably smaller than those in hexane. For example, K_{1-3} of **1a**/Py in THF is 1 order less than that in hexane, and in DCM the value is lower even by 2 orders. These low K_{1-3} values give positive ΔG_{1-3} values, and thus the reaction can be observed only in the presence of a high base excess. Interestingly, the dependence of K_{1-3} (or ΔG_{1-3}) on base is opposite in THF and DCM: HMPA > Py in THF and HMPA < Py in DCM. The last row correlates with the basicity decrease (increase of the conjugated acid K_a), but the sequence in THF corresponds to the decrease of proton-accepting properties in H-bonds (E_j, Table 1).

For several systems in THF, it was possible to determine the proton transfer enthalpy and entropy values (see footnote to Table 9). Both being negative, these values explain the equilibrium shift to the right (Scheme 1) with the temperature

Table 8. Calculated Energies (kcal mol^{-1}) for Hydrogen-Bonded Complexes (HB), Transition States (TS), and Ion Pairs (IP, of the Type **C**) Formed as the Result of Interaction between Hydrides **1** and Bases in Different Media[a]

	1a·Py				**1b**·Py				**1a**·NMe_3				**1b**·NMe_3			
media	ΔE_{HB}	ΔE_{TS}	$\Delta E_{IP(C)}$	ΔE_a[b]	ΔE_{HB}	ΔE_{TS}	$\Delta E_{IP(C)}$	ΔE_a[b]	ΔE_{HB}	ΔE_{TS}	$\Delta E_{IP(C)}$	ΔE_a[b]	ΔE_{HB}	ΔE_{TS}	$\Delta E_{IP(C)}$	ΔE_a[b]
gas phase	−4.8	4.0	−1.0	8.8	−4.4	6.5	1.6	10.9	−5.5	−0.8	−11.1	4.7	−5.2	1.1	−8.8	6.3
heptane	−1.7	5.5	−1.1	7.2	−1.3	7.7	1.7	9.0	−1.7	2.0	−10.5	3.7	−1.2	3.8	−7.8	5.0
THF	−1.0	4.6	−3.0	5.6	−0.5	6.6	0.3	7.1	−1.1	1.6	−12.0	2.7	−0.5	3.4	−8.9	3.9
DCM	−1.1	4.5	−3.0	5.6	−0.6	6.5	0.3	7.1	−1.3	1.5	−12.0	2.8	−0.7	3.2	−9.0	3.9
AN	−1.5	3.4	−4.2	4.9	−1.0	5.4	−0.9	6.4	−1.9	0.5	−13.3	2.4	−1.3	2.2	−10.1	3.5

[a] The energy of the separated neutral reactants (**1** and base) is taken as a zero of energies. The energies in solvent have been obtained by adding the contribution of the free energy of solvation to the gas-phase potential energy. [b] Activation energy: $\Delta E_a = E_{TS} - E_{HB}$.

Table 9. Proton Transfer Equilibrium Constants (K_{1-3}, in L mol^{-1}) and Reaction Free Energies (ΔG_{1-3}, in kcal mol^{-1}) for Interaction of Hydrides **1** with Bases in Different Solvents

		THF 190 K	DCM 190 K	hexane 190 K	hexane 230 K	AN 230 K
			$K_{1-3} = [M^- \cdots {}^+HB]/([MH]\cdot[B])$			
Et_3N	**1b**	4.4×10^4				
HMPA	**1a**	8.4 ± 1.3	$7.1 \pm 1.4 \times 10^{-1}$	53	2.9	35 ± 2
	1b	$1.6 \pm 0.1 \times 10^{-1}$	*a*	23	1.6	$6.6 \pm 1 \times 10^{-1}$
Py	**1a**	1.8 ± 0.2	4.9 ± 1.9	72.4 ± 1.5	*b*	450 ± 30
	1b	*a*	$5.5 \pm 0.5 \times 10^{-2}$	32.2 ± 4.1	*b*	2.0
			ΔG_{1-3}			
Et_3N	**1b**	-4.05 ± 0.07[c]				
HMPA	**1a**	-0.81 ± 0.11[d]	0.14 ± 0.08	-1.49	-1.32	-1.62 ± 0.03
	1b	0.70 ± 0.01	*a*	-1.18	-0.73	0.19 ± 0.07
Py	**1a**	-0.22 ± 0.04[e]	-0.56 ± 0.16	-1.62 ± 0.15	*b*	-2.78 ± 0.03
	1b	*a*	1.09 ± 0.03	-1.31 ± 0.53	*b*	-0.32

[a] No reaction with 200-fold excess of base. [b] No proton transfer at this temperature. [c] $\Delta H_{1-3} = -9.9 \pm 0.4$ kcal mol^{-1}, $\Delta S_{1-3} = -30.8 \pm 1.7$ eu. [d] $\Delta H_{1-3} = -5.1 \pm 0.8$ kcal mol^{-1}, $\Delta S_{1-3} = -22.6 \pm 3.5$ eu. [e] $\Delta H_{1-3} = -2.0 \pm 0.4$ kcal mol^{-1}, $\Delta S_{1-3} = -10.2 \pm 1.7$ eu.

Table 10. Spectroscopic Characteristics of Ion Pairs Involving **3a** and **3b** Formed in Situ in Different Solvents

solvent	**3**	BH^+	ν^sCO[a]	$\Delta\nu_{1/2}{}^s$[b]	$A \times 10^{-4}$[d]	ε_{CO}[c]	$\nu_{CO}{}^{as}$[b]	$\Delta\nu_{1/2}{}^{as}$[b]	$A \times 10^{-4}$[d]	ε_{CO}[c]
AN	**3a**	$^+HNEt_3$	1896	8	*e*	2760	1776	22	*e*	4230
		^+H(HMPA)	1896	8	*e*	*e*	1776	22	*e*	*e*
		^+HPy	1896	8	*e*	*e*	1776	23	*e*	*e*
	3b	$^+HNEt_3$	1890	8	2.8	3367	1771	22	12.3	6000
		^+H(HMPA)	1890	8	*e*	*e*	1771	20	*e*	*e*
		^+HPy	1890	8	*e*	*e*	1771	22	*e*	*e*
THF	**3a**	$^+HNEt_3$	1896 1910 sh	11	2.9	3400	1780 1800 sh, 1770 sh	32	11.1	3700
		^+H(HMPA)	1897	8	*e*	*e*	1779	15	*e*	*e*
		^+HPy	1897[b]				1778	21	*e*	*e*
	3b	$^+HNEt_3$	1888 1902 sh	11	3.4	2800	1777 1796 sh, 1767 sh	30	14.7	3500
		^+H(HMPA)	1891	8	*e*	*e*	1777	17	*e*	*e*
DCM	**3a**	$^+HNEt_3$	1899	18	3.8	1577	1780	44	10.5	2160
		^+H(HMPA)	1894	9	*e*	*e*	1770	*g*		
		^+HPy	*f*		*e*	*e*	1770	*g*		
	3b	$^+HNEt_3$	1891	17	4.0	1511	1774	42	22.3	2018
		^+HPy	*f*		*e*	*e*	1765	31	*e*	*e*

[a] In cm^{-1}. [b] Half-height full widths, $\Delta\nu_{1/2}$, in cm^{-1}. [c] Molar extinction coefficients in L mol^{-1} cm^{-1}. [d] Integral intensity in L mol^{-1} cm^{-2}. [e] Partial proton transfer. [f] Overlapped with the Py band. [g] Low intensity of the band precludes reliable measurement.

decrease. On the other hand, the entropy term is rather high, so it makes the reaction free energy positive for **1a** with Py above 200 K and with HMPA above 230 K.

Thus, the solvent effect observed is in agreement with that predicted by CPCM calculations only for the extreme cases of nonpolar hexane and polar acetonitrile. Medium polarity solvents, which feature significant ability to form HB, give proton transfer constants lower than those in nonpolar hexane. We believe this effect could be explained considering the specific solute−solvent interactions.

2.3.3. Solvent Effect on Proton Transfer: Ion Pairing. As is well-known, depending on the solvent polarity, the ionic species could exist as solvent separated ion pairs or contact ion pairs.[68,70] In acetonitrile, the most polar solvent used in this study (ε = 47.56 at 230 K), the position and half-height full width, $\Delta\nu_{1/2}$, of the ν_{CO} bands of both anions **3a** and **3b** are independent of the cation (Table 10). Interestingly, the $\Delta\nu_{1/2}$ values are similar to those of the ν_{CO}(**1**) bands (Table 7). These data show the absence of the structural perturbation and prove formation of solvent separated ion pair. In contrast, the characteristics of the ν_{CO} bands of **3a** and **3b** formed by interaction of **1** with bases (Table 10) in DCM and THF are different. Comparison of the data in these solvents with those in AN shows that ν_{CO} bands (especially the low frequency $\nu_{CO}{}^{as}$) are sensitive to the solvent and the counterion. Thus, IR spectra for **3**/NEt_3H^+ obtained in situ in THF reveal new high and low frequency shoulders similar to the reported spectra of tetramethylammonium cation with $CpMo(CO)_3$ anion in THF.[53] The $\Delta\nu_{1/2}$ values are lower for ion pairs with $[HPy]^+$ and minimal for protonated HMPA. Such a dependence is typical for contact ion pairs and could be explained by the different number and strength of additional interactions between carbonyls of the anion and CH groups of cations. In the case of DCM, the $\nu_{CO}{}^{as}$(**3**) bands are the broadest among those observed, as for the starting complexes **1**. Although frequency changes are not large, the same was observed early for contact ion pairs with alkali metals.[53] Thus, in all solvents studied, except AN, the products of proton transfer from hydrides **1** to bases exist as contact ion pairs stabilized by H-bonding between organometallic anion and organic cation. Combined with the frequency calculation results, the spectroscopic data suggest that ion pairs have structure **C** (Figure 9) with cation located opposite to the Cp ring of the anion.

Discussion

The study presented is the first complete investigation of the solvent effect on the metal hydrides interaction with bases. The complexes studied, $CpMH(CO)_3$ (**1**), behave as weak hydrogen-

(69) Belkova, N. V.; Besora, M.; Epstein, L. M.; Lledós, A.; Maseras, F.; Shubina, E. S. *J. Am. Chem. Soc.* **2003**, *125*, 7715–7725.
(70) Macchioni, A. *Chem. Rev.* **2005**, *105*, 2039–2074.

Scheme 2. Hydrogen Bonding with Protic (SH) and Aprotic, Proton-Accepting (S) Solvents

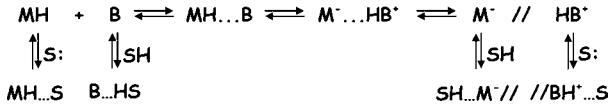

bond donors forming MH···base hydrogen-bonded adducts of the energy similar to those of CH-donors. Comparable energies of MH···base and MH···S (S = THF or AN) hydrogen bonds make them competitive and difficult, if at all possible, to observe spectroscopically the former. This could be the likely cause of the failure to find MH···base hydrogen bonds in the case of $HCo(CO)_4$.[71] In this section, we would like to consider the peculiarities of MH systems in comparison to CH or traditional OH/NH proton donors and the role of nonspecific and specific interactions with the media at different stages of the proton transfer equilibrium (Scheme 2).

The hydrides **1** feature pK_a values (13.9 and 16.1 in CH_3CN for **1a** and **1b**, respectively) that are significantly lower than those of the CH groups (pK_a = 50 for C_2H_6, 44 for C_2H_4, 25 for C_2H_2, 32 for Ph_3CH). This difference is probably due to the rather low energy of the M−H bond:[72] BDE of **1a** is 66[75] to 70[5] kcal mol^{-1}, of **1b** is 73[5] kcal mol^{-1}, whereas BDE of C−H varies from, for example, 92−104 kcal mol^{-1} in $(CH_3)_{3-n}H_nCH$ (n = 0−3) to 81 kcal mol^{-1} in Ph_3CH.[76] M−H bond polarization increases easily in the presence of base (at notably lower interaction energies than in the case of C−H bonds; see Figure 6) that in turn facilitates $M^{\delta-}-H^{\delta+}$ heterolytic splitting. Thus, the deprotonation of hydrides **1** occurs readily, placing these complexes between medium strength OH proton donors on the pK_a(CH_3CN) scale (compare, for example, to pK_a(CH_3CN) 20.55 of $(CF_3)_3COH$, 16.66 of 2,4-dinitrophenol, or 11.00 of 2,4,6-trinitrophenol[77]). On the other hand, OH proton donors do not transfer proton to a base in the nonpolar media even at much higher hydrogen-bonded complex strength. For example, a 4-nitrophenol/Et_3N mixture exists as an ion pair in CH_3CN but as a hydrogen-bonded molecular complex with $\Delta H_{HB}^{\circ} = -9.3$ kcal mol^{-1} in *i*-octane.[78] In contrast, the enthalpy of the hydrogen bond between **1** and bases is only about −3 kcal mol^{-1} in hexane, but proton transfer does occur in this solvent.

Another peculiarity of $CpMH(CO)_3$ as a proton donor is a high d-electron lone pair delocalization (according to the NBO analysis). Thus, the possibility to form conjugated systems XH···MH···base (analogous to those in eq 2), which would strengthen the hydrogen-bonded complex and promote proton transfer, is lacking. Therefore, the position of the tautomeric equilibrium M−H···B ⇄ M^-···$^+$HB (central part in Scheme 2) could be affected only by media polarity. As is clearly evidenced by the experimental data, the substantial polarity increase on going from hexane to acetonitrile shifts the overall equilibrium to the right, toward the proton transfer product.

On the other hand, the proton transfer equilibrium constants, K_{1-3}, and the reaction free energies are lower in medium polarity solvents (DCM, THF) than in hexane. The data obtained suggest that the key to understanding this phenomenon lies in specific solute−solvent interactions. The CH···OC interaction between **1** and the media is evidently present even in those solvents that are traditionally considered as proton acceptors (THF, AN). In turn, the hydrogen-bond-donating CH_2Cl_2 interacts not only with carbonyl ligands of **1** but with bases. According to our experimental and computational results, both CH···base and M−H···X interactions (X = N of acetonitrile or O of THF) have energy comparable to that of the M−H···base hydrogen bond. Thus, these competitive interactions lower hydride or base activity in the proton transfer reaction and in this way affect the position of the proton transfer equilibrium (Schemes 1 and 2).

Formation of homoconjugated cations $[BHB]^+$, which is feasible under the large base excess used, would lead to the hydrogen-bonded ion pair M^-···$^+$HB dissociation as would the BH^+ interaction with proton-accepting and M^- interaction with proton-donating solvents. Yet the interactions between charged partners of ion pairs should be stronger than ion−molecular interactions with solvents. Therefore, the influence of specific solvation of ionic species (right-hand side of Scheme 2) on the position of the proton transfer equilibrium should be less profound than that of the reagents (left-hand side of Scheme 2). Indeed, the order of the proton transfer equilibrium constants and reaction free energies as a function of solvent contrasts the order of the ion pair stability (the reaction thermodynamics) obtained by CPCM calculations. This indicates that the hampering effect of specific solvation (hydrogen bonding) of neutral reactants on the proton transfer is more important than the solvent polarity increase.

Conclusion

Despite the unusual nature of neutral transition metal hydrides as hydrogen-bond donors, their MH···base complexes have structural, electronic, and energetic features, which resemble those of CH···base hydrogen bonds of similar strength. However, despite the low MH···base hydrogen-bond formation energy, the proton transfer and ionic form formation take place in these systems even in nonpolar media. This process is found to be assisted by low temperature or high base excess. Such reactivity pattern contrasts not only the behavior of CH proton donors but that of classical organic systems of similar strength. Thus, the easiness of proton transfer appears to be a general peculiarity of proton transfer reactions involving transition metal hydrides as either acids or bases.[79] In both cases, this could be due to the lower energy of an M−H bond and better delocalization of the acquired charge (negative or positive) in the presence of transition metal in comparison to traditional organic bases. Easy deprotonation makes the MH···base complexes the most reasonable intermediates of (catalytic) processes involving H^+ transfer from transition metal hydrides.

An important consequence of the low strength of M−H···B interaction is high sensitivity of the proton transfer equilibrium to the environment. In the case of low (medium) polarity

(71) Kristjánsdóttir, S. S.; Norton, J. R.; Moroz, A.; Sweany, R. L.; Whittenburg, S. L. *Organometallics* **1991**, *10*, 2357–2361.
(72) For the linear relationship of BDE and pK_a and the thermodynamic cycle behind that, see, for example, refs 5, 73, and 74.
(73) Jaun, B.; Schwarz, J.; Breslow, R. *J. Am. Chem. Soc.* **1980**, *102*, 5741.
(74) Nicholas, A. M. d. P.; Arnold, D. R. *Can. J. Chem.* **1982**, *60*, 2165.
(75) Nolan, S. P.; Lopez de la Vega, R.; Hoff, C. D. *Organometallics* **1986**, *5*, 2529–2537.
(76) Luo, Y.-R. *Handbook of Bond Dissociation Energies in Organic Compounds*; CRC Press: Boca Raton, FL, 2003; p 392.
(77) Kuejtt, A.; Leito, I.; Kaljurand, I.; Soovaeli, L.; Vlasov, V. M.; Yagupolskii, L. M.; Koppel, I. A. *J. Org. Chem.* **2006**, *71*, 2829–2838.
(78) Baba, H.; Matsuyama, A.; Kokubun, H. *Spectrochim. Acta, Part A* **1969**, *25*, 1709–1722.
(79) Belkova, N. V.; Epstein, L. M.; Shubina, E. S. *ARKIVOC* **2008**, *iv*, 120–138.

solvents, the specific solute−solvent interactions have a profound hampering effect, which overcomes the effect of the solvent polarity increase upon transition from nonpolar media. This phenomenon could be equally important for any weakly bound acid−base system.

Acknowledgment. Financial support from the Russian Foundation for Basic Research (project no. 08-03-00464-a), the Division of Chemistry and Material Sciences of the Russian Academy of Sciences, and the Russian Federation President grant (MK-314.2010.3) is gratefully acknowledged. A.L. thanks the Spanish MICINN (Projects CTQ2008-06866-CO2-02 and Consolider_Ingenio 2010 CSD2007-00006). CESCA is acknowledged for providing computational resources.

Supporting Information Available: IR spectra, complete ref 30, details of the AIM analysis, and Cartesian coordinates for the optimized geometries of the calculated species. This material is available free of charge via the Internet at http://pubs.acs.org.

JA103862R